SAND89-2425C
Proposed for presentation at the 5th
AIAA/ASME Conference, June 18-20, 1990
Seattle, WA
CONF-900619--1

Heat-Transfer Regimes in Nuclear-Reactor-Pumped Gas Lasers*

J. R. Torczynski

Fluid and Thermal Sciences Department

Sandia National Laboratories

Albuquerque, NM 87185-5800

SAND--89-2425C

DE90 002904

The flow induced in nuclear-reactor-pumped gas lasers by the competing effects of spatially nonuniform fission-fragment heating (pumping) and heat transfer to the walls is examined. The equations of motion are acoustically filtered (low Mach number approximation), and the resulting equations are seen to have three timescales: the duration of the heating, the time required by the heating to produce a pressure rise comparable to the initial pressure, and the time for the thermal boundary layer to grow into the center of the laser cell. Three distinct regimes emerge from consideration of the relative magnitudes of these timescales. In the negligible-conduction regime, thermal-conduction effects are small, and the motion is determined by the spatial nonuniformity of the heating. In the dominant-conduction regime, thermal-conduction effects govern the motion. In the mixed regime, the effects of thermal conduction and heating nonuniformity are comparable, but since they are oppositely directed, a complex gas motion results. Analytical solutions to the equations of motion are presented for the negligible-conduction and dominant-conduction regimes, and examples are given for all three regimes. Plots of the second spatial derivative of the density field (a quantity often used in optical analyses) are given for the negligible-conduction and the dominant-conduction regimes as functions of the appropriate similarity parameters.

*This work was performed at Sandia National Laboratories, supported by the U. S. Department of Energy under contract number DE–AC04–76DP00789.

DISCLAIMER

Nomenclature

c_p	specific heat at constant pressure
c_v	specific heat at constant volume
e	energy per unit mass
G	spatial variation of applied heating
h	temporal variation of applied heating
k	thermal conductivity
k_0	initial thermal conductivity
$\tilde{k}$	k/k_0 (nondimensional)
L	domain semi-extent in x
p	pressure
p_0	initial pressure
$\bar{p}$	x-averaged p
$\hat{p}$	$p - \bar{p}$
$\tilde{p}$	$\bar{p}/p_0$ (nondimensional)
Q	volumetric applied heating
Q_*	amplitude of applied heating
$\tilde{Q}$	Q/Q_* (nondimensional)
R	gas constant
S_A	amplitude similarity parameter
S_B	boundary layer similarity parameter
S_B^*	S_B value when $t_D \approx t_C$
S_F	foil-thickness similarity parameter
S_H	homogeneity similarity parameter
S_Q	heating similarity parameter
t	time
t_C	thermal-conduction timescale

t_D	heating duration
$\tilde{t}$	t/t_D (nondimensional)
T	temperature
T_0	initial temperature
$\tilde{T}$	T/T_0 (nondimensional)
u	velocity x-component
$\tilde{u}$	ut_D/L (nondimensional)
x	Cartesian coordinate (across width)
$\tilde{x}$	x/L (nondimensional)
$\tilde{x}_0$	Lagrangian parametric variable
α	thermal conductivity exponent
γ	specific heat ratio
κ	thermal diffusivity $k_0/\rho_0 c_v$
μ	shear viscosity
μ_0	initial shear viscosity
$\tilde{\mu}$	μ/μ_0 (nondimensional)
μ_v	bulk viscosity
$\tilde{\mu}_v$	μ_v/μ_0 (nondimensional)
$\tilde{\pi}$	$\hat{p}t_D^2/\rho_0 L^2(1+S_B)$ (nondimensional)
ρ	density
ρ_0	initial density
$\tilde{\rho}$	ρ/ρ_0 (nondimensional)
ξ	dummy variable

Introduction

It is possible to pump gas lasers with the energetic products of fission reactions (fission fragments) induced by a pulse of neutrons from a nuclear reactor.[1-10] Such "nuclear-reactor-pumped" lasers have some important advantages over lasers with other pumping methods. First, the nuclear energy is utilized directly to excite atomic or molecular lasing states. The alternative to this is conversion of the nuclear energy to heat and subsequently to electricity (with the associated efficiency losses at each conversion) before being used to excite the laser medium.[11] Second, these lasers can take advantage of the large energy densities associated with nuclear power.[11]

Figure 1 shows a schematic diagram of a laser cell which illustrates one means by which this type of pumping can be achieved. When irradiated with the neutron flux from a nuclear

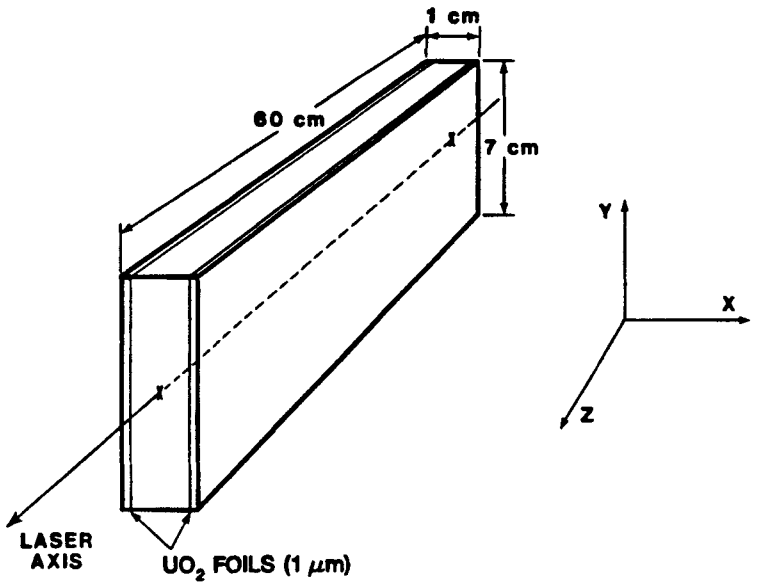

Figure 1. Schematic diagram of a typical laser cell used in nuclear-reactor-pumped-laser research.

reactor, coatings of fissionable material on the side walls of the laser cell emit fission fragments. Some of these fission fragments pass through the gas-filled region of the laser cell, depositing energy as they go. Since most of the deposited energy is rapidly thermalized, the pumping process heats the gas. This heating is large (the energy deposited in the gas during

the pulse is comparable to the thermal energy originally present), transient (the neutron flux varies temporally), spatially nonuniform (the fission fragments heat the gas more near the side walls), and volumetric (the fission fragments penetrate deeply into the gas to deposit energy). The spatial nonuniformity of the applied heating induces gas motion in toward the center (laser optical axis). However, the side walls remain colder than the gas, so heat-transfer effects induce gas motion out toward the walls. Since these effects are oppositely directed, heat-transfer and heating-nonuniformity effects compete to determine the overall gas motion.

Since the density of a gas is related to its refractive index,[12] this gas motion establishes gradients in the refractive index normal to the optical axis. More specifically, the heated gas acts like a lens with a temporally varying focal length. Under certain circumstances, the lensing produced in this manner can change the optical stability of the laser resonator.[13–15] Thus, in order to predict the optical behavior of these lasers, it is essential to understand the gas motion induced by the competing effects of the thermal conduction and the heating nonuniformity.

Previous studies have concentrated on the gas motion induced by the spatial nonuniformity of the fission-fragment heating but have neglected the effect of thermal conduction on the gas motion.[16–20] Although this is justified for short pulses during which the effects of thermal conduction are confined to thin thermal boundary layers at the side walls, for longer pulses this assumption breaks down. In this paper, the gas motion in a nonuniformly heated laser medium is analyzed including the effects of heat transfer to the cold side walls. Three heat-transfer regimes are found. Analytical solutions for the induced gas flow are presented for two of the regimes, and examples are presented for all three regimes.

The Model Problem

In order to understand the laser's optical behavior, the following model describing the gas motion is examined. The gas is assumed to obey the perfect gas law,

$$p = R\rho T \ , \tag{1}$$

where p, ρ, T, and R are the pressure, density, temperature, and gas constant, respectively. The gas is also assumed to have constant specific heats c_p and c_v, with the ratio $\gamma = c_p/c_v$ thus constant. The thermal conductivity of the gas is assumed to vary with temperature according to the relation

$$k = k_0(T/T_0)^\alpha \ , \tag{2}$$

where k_0, T_0, and α are constants. This relation, although approximate, provides a relatively accurate representation of the thermal conductivity of many gases.[21]

Flow and variation of thermodynamic properties are allowed only in the x-direction (see Figure 1). Thus, this model neglects variations in the y- and z-directions. Such variations are often minor;[13,20] moreover, the emphasis of this paper is on heating-nonuniformity and thermal-conduction effects, which are strongest in the x-direction. The values $x = \pm L$ and $x = 0$ are chosen to correspond to the side walls and to the centerplane (in which the laser optical axis lies), respectively, and symmetry about $x = 0$ is assumed henceforth.

The equations describing the gas motion are the conservation equations for mass, momentum in the x-direction, and energy:

$$\frac{\partial \rho}{\partial t} + \frac{\partial}{\partial x}\rho u = 0 \ , \tag{3}$$

$$\frac{\partial}{\partial t}\rho u + \frac{\partial}{\partial x}\rho u^2 = -\frac{\partial p}{\partial x} + \frac{\partial}{\partial x}\left[\left(\frac{4}{3}\mu + \mu_v\right)\frac{\partial u}{\partial x}\right] \ , \tag{4}$$

$$\begin{aligned} &\frac{\partial}{\partial t}\rho\left(e + \tfrac{1}{2}u^2\right) + \frac{\partial}{\partial x}\rho u\left(e + p/\rho + \tfrac{1}{2}u^2\right) \\ &= Q + \frac{\partial}{\partial x}\left(k\frac{\partial T}{\partial x}\right) + \frac{\partial}{\partial x}\left[u\left(\frac{4}{3}\mu + \mu_v\right)\frac{\partial u}{\partial x}\right] \ , \end{aligned} \tag{5}$$

$$e = p/\rho(\gamma - 1) \ . \tag{6}$$

Here, u, μ, μ_v, e, and Q are the velocity, the shear viscosity, the bulk viscosity, the energy per unit mass, and the applied power density from fission-fragment heating, respectively. By virtue of the assumed symmetry, only the region from $x = 0$ to $x = L$ is considered. Boundary conditions for these equations are $u = 0$ at $x = 0$ and $x = L$, $T = T_0$ at $x = L$, and $\partial T/\partial x = 0$ at $x = 0$.

The energy equation has a source term Q on the right-hand side corresponding to fission-fragment heating. This volumetric heat source has the form

$$Q = Q_s h(t/t_D) L \frac{\partial}{\partial x} G\left(\frac{1}{L}\int_0^x \frac{\rho(x',t)}{\rho_0}\,dx'; S_H, S_F\right)$$

$$= Q_s h(t/t_D)\left(\frac{\rho}{\rho_0}\right) G'\left(\frac{1}{L}\int_0^x \frac{\rho(x',t)}{\rho_0}\,dx'; S_H, S_F\right) . \qquad (7)$$

Although Equation (7) is daunting at first sight, the quantities in this equation all have straightforward interpretations. The quantity Q_s is the scale factor which converts the (nondimensional) neutron flux $h(t/t_D)$ into power density (kW/cm^3). The function h is the temporal variation of the neutron flux, which is approximately Gaussian, and t_D is the timescale characterizing the duration of the neutron pulse, proportional to the full width at half maximum. The term $\partial G/\partial x$ is the spatial variation of the applied heating. The derivative $\partial/\partial x$ appears since the energy source term is the divergence of the corresponding nondimensional fission-fragment energy flux (G). The argument of G represents the coupling between the gas density field and fission-fragment energy deposition.[20,22-24] Since the absorption of fission-fragment energy depends on the number of absorbers (molecules) present per unit volume, the gas density appears in an integral in the argument of G, which is similar to its appearance in the related problem of light absorption by a gas. The function G is monotonically increasing with positive concavity, and the normalization of G is chosen conveniently to yield $G(0) = 0$ and $G(1) = 1$ (see Figure 2). Calculation of the x-variation of Q from Equation (7) gives a roughly parabolic profile proportional to G' which is concave upward and has a minimum at $x = 0$ (see Figure 2). The quantities S_H and S_F are model-dependent similarity parameters[20] determining the precise form of the spatial variation of Q. As the homogeneity similarity parameter S_H is increased, the minimum for Q becomes deeper, and when $S_H = 0$, Q has no spatial variation. Thus, S_H is a measure of how homogeneous or spatially uniform the applied heating is. The foil-thickness similarity parameter S_F has relatively little effect on the shape of Q and will not be discussed further. See Ref. 20 for a detailed discussion of Q.

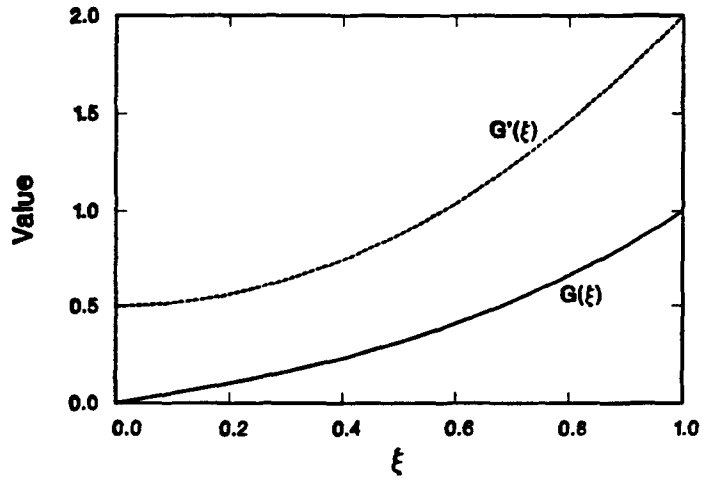

Figure 2. Typical examples of $G(\xi)$ (solid curve) and $G'(\xi)$ (dashed curve), the slope of G. $G'(\xi)$ indicates the spatial variation of the applied heating.

There are several relevant timescales in this model: the time for an acoustic wave to travel from the side walls to the center; the time for thermal-conduction effects to reach the center from the side walls; the time over which the energy is deposited (the pulse duration); and the time required for the applied heating to increase the pressure and temperature by amounts comparable to their initial values. Typically, the acoustic timescale is much smaller than the other three timescales, so the Mach number of the induced flow is much less than unity. Therefore, the equations can be acoustically filtered.[20,25,26] This procedure has the effect of removing the wave nature of the pressure variation from the problem: the pressure partitions into a large mean $\bar{p}(t)$ plus a small local deviation $\hat{p}(x,t) = p(x,t) - \bar{p}(t)$. Thus, acoustic filtering effectively removes the acoustic timescale from consideration. The equations that result from this procedure are:

$$\frac{\partial \rho}{\partial t} + \frac{\partial}{\partial x}\rho u = 0 \,, \tag{8}$$

$$\frac{\partial}{\partial t}\rho u + \frac{\partial}{\partial x}\rho u^2 = -\frac{\partial \hat{p}}{\partial x} + \frac{\partial}{\partial x}\left[\left(\frac{4}{3}\mu + \mu_v\right)\frac{\partial u}{\partial x}\right] \,, \tag{9}$$

$$\frac{d\bar{p}}{dt} = (\gamma - 1)Q_* h(t/t_D) + \frac{(\gamma - 1)}{L}\left(k\frac{\partial T}{\partial x}\right)\Big|_{x=L} \,, \tag{10}$$

$$\gamma\bar{p}u = (\gamma-1)Q_*h(t/t_D)L\left[G\left(\frac{1}{L}\int_0^x \frac{\rho(x',t)}{\rho_0}\,dx'\right) - \frac{x}{L}\right] + (\gamma-1)\left[k\frac{\partial T}{\partial x} - \frac{x}{L}\left(k\frac{\partial T}{\partial x}\right)\Big|_{x=L}\right], \tag{11}$$

$$\bar{p} = R\rho T\,. \tag{12}$$

The general procedure to obtain these equations is outlined in Ref. 20 although the thermal-conduction and viscous terms are not included in that study.

These equations have the following physical interpretations. Equations (8) and (9) are just mass and momentum conservation (since $\bar{p}$ is not a function of x, it does not appear in Equation (9)). Equations (10) and (11) are related to energy conservation. Equation (10) shows that the mean pressure rise is governed by the mean heat addition minus the mean heat loss by thermal conduction (it is the perfect gas law in an unusual form). Equation (11) shows that velocities are induced when the local heating (both applied and conduction) differs from the mean heating (shown in Equation (10)). Thus, the tendency is for the system to approach uniform heating.[20] Note that $\hat{p}$ appears only in Equation (9), so in effect it is decoupled from the motion.

To assess different flow and heat-transfer regimes, it is necessary to cast these equations in nondimensional form. The following nondimensionalization is used:

$$\begin{array}{llll} \tilde{\rho} = \rho/\rho_0 & \tilde{p} = \bar{p}/p_0 \\ \tilde{T} = T/T_0 & \tilde{k} = k/k_0 \\ \tilde{x} = x/L & \tilde{t} = t/t_D & , \\ \tilde{u} = ut_D/L & \tilde{\pi} = \hat{p}t_D^2/\rho_0 L^2(1+S_B) \\ \tilde{\mu} = \mu/\mu_0 & \tilde{\mu}_v = \mu_v/\mu_0 \end{array}$$

where S_B will be defined shortly. The equations that result from this procedure are:

$$\tilde{p} = \tilde{\rho}\tilde{T}\,, \tag{13}$$

$$\tilde{k} = \tilde{T}^{\alpha}\,, \tag{14}$$

$$\frac{\partial\tilde{\rho}}{\partial\tilde{t}} + \frac{\partial}{\partial\tilde{x}}\tilde{\rho}\tilde{u} = 0\,, \tag{15}$$

$$S_A^{-1}\frac{d\tilde{p}}{d\tilde{t}} = h(\tilde{t}) + S_Q^{-1}\left(\tilde{k}\frac{\partial\tilde{T}}{\partial\tilde{x}}\right)\Big|_{\tilde{x}=1}\,, \tag{16}$$

$$S_A^{-1}\gamma\tilde{p}\tilde{u} = h(\tilde{t})\left[G\left(\int_0^{\tilde{x}}\tilde{\rho}\,d\tilde{x}'\right) - \tilde{x}\right] + S_Q^{-1}\left[\tilde{k}\frac{\partial\tilde{T}}{\partial\tilde{x}} - \tilde{x}\left(\tilde{k}\frac{\partial\tilde{T}}{\partial\tilde{x}}\right)\Big|_{\tilde{x}=1}\right], \tag{17}$$

$$\frac{\partial}{\partial\tilde{t}}\tilde{\rho}\tilde{u} + \frac{\partial}{\partial\tilde{x}}\tilde{\rho}\tilde{u}^2 = -(1+S_B)\frac{\partial\tilde{\pi}}{\partial\tilde{x}} + S_B\left(\frac{\mu_0 c_p}{\gamma k_0}\right)\frac{\partial}{\partial\tilde{x}}\left[\left(\frac{4}{3}\tilde{\mu} + \tilde{\mu}_v\right)\frac{\partial\tilde{u}}{\partial\tilde{x}}\right]. \tag{18}$$

Here, the parameters S_A, S_Q, and S_B are defined as follows:

$$S_A = \frac{(\gamma-1)Q_s t_D}{p_0}, \tag{19}$$

$$S_Q = \frac{Q_s L^2}{k_0 T_0}, \tag{20}$$

$$S_B = \frac{(\gamma-1)k_0 T_0 t_D}{p_0 L^2}. \tag{21}$$

The amplitude similarity parameter S_A is the ratio of the pulse duration to the pressure-rise timescale and as such indicates the scale of the normalized pressure rise that would be produced by the applied heating in the absence of thermal conduction. The heating similarity parameter S_Q is proportional to the ratio of the thermal-conduction timescale (the time required for the thermal boundary layers to grow from the side walls into the center of the laser cell) to the pressure-rise timescale and therefore measures the relative strength of the applied heating to thermal-conduction loss. The boundary layer similarity parameter S_B is proportional to the ratio of the pulse duration to the thermal-conduction timescale. Note that these parameters are not independent but obey the relation

$$S_A = S_B S_Q. \tag{22}$$

Since in the notation of Carslaw and Jaeger[27] the thermal-conduction timescale t_C can be estimated using a value of $x/2\sqrt{\kappa t_C} \approx 2$ with $x = L$ and $\kappa = k_0/\rho_0 c_v$, the thermal-conduction timescale t_C and the pulse duration t_D are approximately equal when $S_B = S_B^* \approx 1/16$. Thus, S_B^* is the reference value to which S_B is to be compared to determine the relative importance of thermal-conduction and heating-nonuniformity effects.

The type of motion that results from the equations of motion is governed by the relative values of these parameters. This behavior can be determined through application of the principle of dominant balance.[28] Simply put, the largest terms in these equations must be approximately equal, and smaller terms can be neglected. In each of Equations (16) and (17) there are three terms: a "source" term involving h; a "loss" term involving thermal conduction scaled by S_Q^{-1}; and a "dynamic-response" term scaled by S_A^{-1}. Since this study emphasizes motion induced by the applied heating, the source term must be balanced by (at least) one of the other two terms. [By way of contrast, the cool-down period following the termination of heating is *not* considered herein.] Suppose $S_B/S_B^* \ll 1$. Then by Equation (22) terms proportional to S_A^{-1} are much larger than terms proportional to S_Q^{-1}, so the balance is between the source terms and the dynamic-response terms. This is the negligible-conduction regime. Suppose $S_B/S_B^* \gg 1$. Then by Equation (22) terms proportional to S_A^{-1} are much smaller than terms proportional to S_Q^{-1}, so the balance is between the source terms and the loss terms. This is the dominant-conduction regime. Suppose $S_B/S_B^* \sim 1$. Then by Equation (22) all terms are of the same magnitude, so no terms can be removed from the equations. This is the mixed regime. In the following sections, each regime is considered in turn.

Negligible-Conduction Regime

In the negligible-conduction regime ($S_B/S_B^* \ll 1$), thermal-conduction effects are confined to thin boundary layers at the side walls. The total heat removed from the gas by thermal conduction over the duration of the pulse is thus very small and does not affect the gas motion significantly. In the limit $S_B \to 0$, the equations have the following solution in Lagrangian parametric form:[20]

$$\tilde{p} = 1 + S_A \int_{-\infty}^{\tilde{t}} h(\tau)\, d\tau \ , \tag{23}$$

$$\tilde{\rho} = \left\{ G'(\tilde{x}_0) + [1 - G'(\tilde{x}_0)]\tilde{p}^{-1/\gamma} \right\}^{-1} \ , \tag{24}$$

$$\tilde{x} = G(\tilde{x}_0) + [\tilde{x}_0 - G(\tilde{x}_0)]\tilde{p}^{-1/\gamma} \ , \tag{25}$$

$$G'(\xi) = \frac{dG}{d\xi} \ . \tag{26}$$

In these equations, the parametric variable $\tilde{x}_0$ must be eliminated to find the spatial variation of the density field $\tilde{\rho}(\tilde{x},\tilde{t})$. Although previously derived,[20] the solution for this regime is presented here to illustrate its region of validity ($S_B/S_B^* \ll 1$) and to contrast this regime with the other regimes. Note that S_A is the important similarity parameter in this regime.

From the above equations, it is seen that the gas density distribution at a given time is determined by the normalized pressure at that time, where the normalized pressure is just the normalized amount of energy in the gas at that time (see Equation (23)). By way of contrast, the heating rate (proportional to h) is unimportant since it enters only in an integral sense in Equation (23). Since the quantity $\tilde{x}_0 - G(\tilde{x}_0)$ is positive (see Figure 2), the induced gas flow is inward and improves the spatial uniformity of the applied heating (absorbers move into the low-flux region near $x = 0$ and out of the high-flux region near $x = L$). A density maximum is thus produced in the center, so the heated region is optically focusing. Note also that as $\tilde{p}$ (or equivalently S_A) becomes large, the density field approaches a limiting profile, which is unaffected by further heat addition. Analytical results for $\tilde{u}$, $\tilde{\pi}$, and other quantities are contained in the appendix.

As an example, consider helium gas, initially at 200 kPa and 300 K, contained in a laser cell with a 1-cm gap ($L = 0.5$ cm) and with 1-μm UO_2 layers on the side walls. The heating is described by $Q_s = 3.55$ kW/cm^3 and $h = 1$ for $0 \le t \le t_D$ with $t_D = 0.1$ ms ($h = 0$ at other times). For this case, $S_B/S_B^* = 0.0095$. Figures 3 and 4 show the spatial variations of the density and power density (applied heating) fields, respectively, at 0.05 ms and 0.1 ms as determined from a numerical simulation of the full equations. Outside the thin thermal boundary layers, the gas motion is inward, as discussed above. Also, the applied heating has become slightly more uniform at later times.

The quantity $\partial^2\tilde{\rho}/\partial\tilde{x}^2(0)$, often used in optical stability analyses of laser resonators,[13-15] can be determined for the negligible-conduction regime. In the limit $S_B \to 0$ with

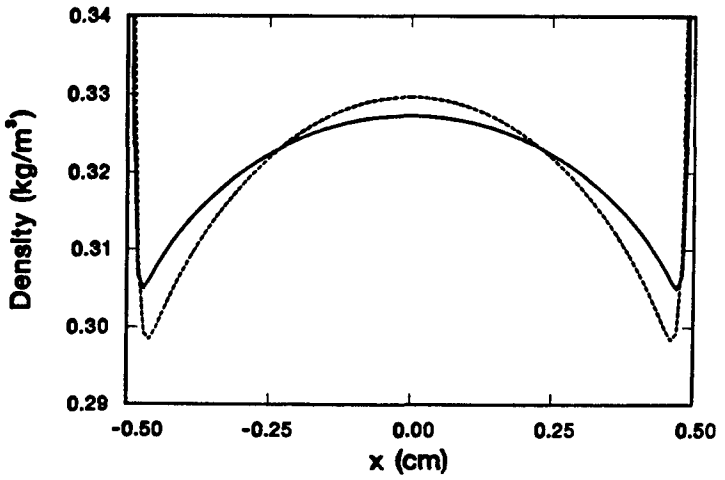

Figure 3. The density is shown as a function of position at 0.05 ms (solid curve) and 0.1 ms (dashed curve). Note the inward gas motion and the thin thermal boundary layers.

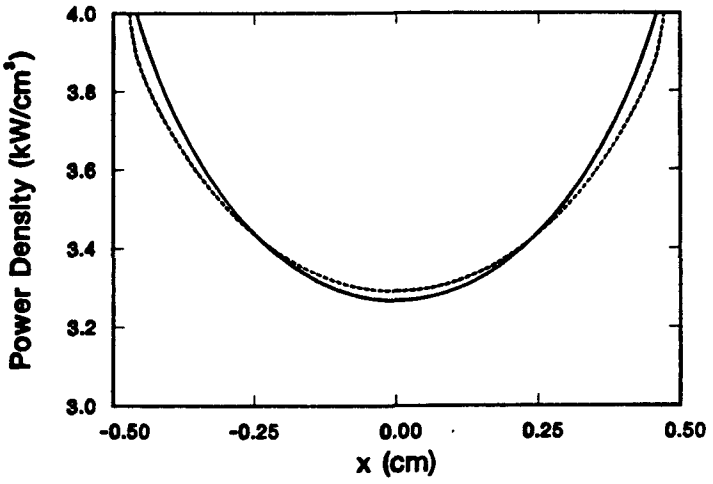

Figure 4. The power density (heating) is shown as a function of position at 0.05 ms (solid curve) and 0.1 ms (dashed curve). Note the increased uniformity at the later time.

$\int_{-\infty}^{\infty} h(\tau)\, d\tau = 1$, this quantity can be expressed as

$$\frac{\partial^2 \tilde{\rho}}{\partial \tilde{x}^2}(0) = r_1(S_H, S_F)\, r_2(S_A, S_H, S_F)\ . \tag{27}$$

Plots of r_1 and r_2 are given in Figures 5 and 6. These generic plots can be used to determine the amount of lensing to be expected for experiments lying in the negligible-conduction regime. From these graphs, it is seen that larger values of S_A and S_H produce larger

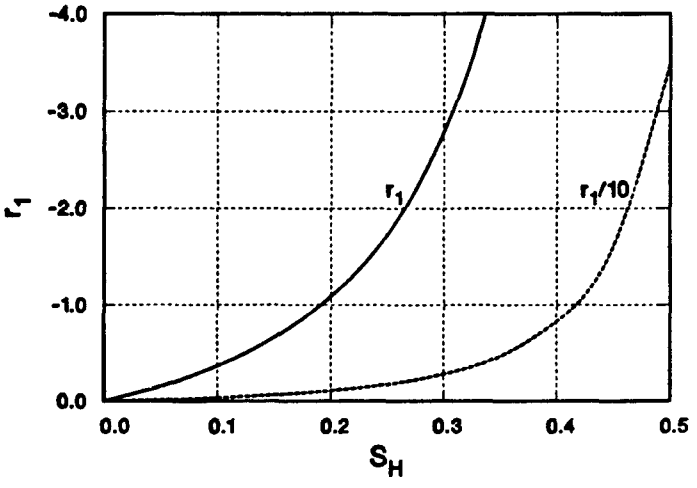

Figure 5. The quantity r_1 is plotted against S_H for $S_F = 0.2$ (solid curve is full scale, dashed curve has been reduced by a factor of ten for convenience of display). These results depend very weakly on S_F.

curvatures of the density field. These observations are summarized by the statement that large heating (large S_A) and large nonuniformity (large S_H) produce large motion.

Dominant-Conduction Regime

In the dominant-conduction regime ($S_B/S_B^* \gg 1$), thermal conduction affects the gas flow everywhere and removes heat as rapidly as it is deposited. In the limit $S_B \to \infty$, the equations have the following solution in Lagrangian parametric form:

$$\tilde{p} = \int_0^1 \{1 + [H(1) - H(\xi)]\alpha S_Q h/\tilde{p}\}^{1/\alpha}\, d\xi\ , \tag{28}$$

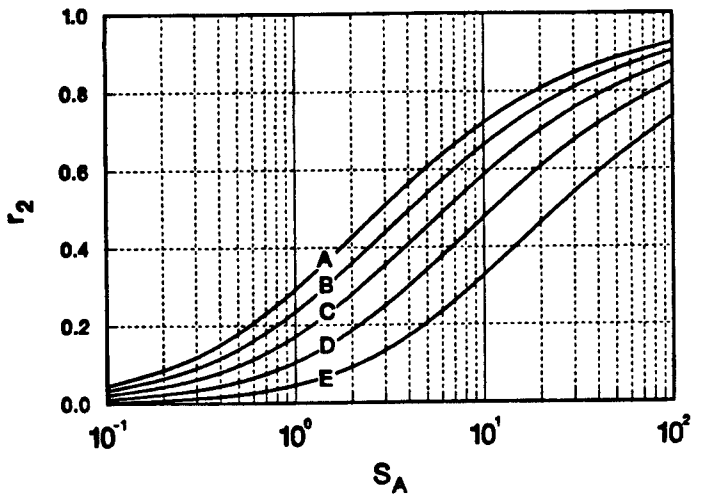

Figure 6. The quantity r_2 is plotted against S_A for $S_F = 0.2$ and the following S_H values: $S_H = 0.1$ (curve A); $S_H = 0.2$ (curve B); $S_H = 0.3$ (curve C); $S_H = 0.4$ (curve D); $S_H = 0.5$ (curve E). These results depend very weakly on S_F.

$$\tilde{\rho} = \tilde{p}\,\{1 + [H(1) - H(\tilde{x}_0)]\alpha S_Q h/\tilde{p}\}^{-1/\alpha} \ , \tag{29}$$

$$\tilde{x} = \tilde{p}^{-1} \int_0^{\tilde{x}_0} \{1 + [H(1) - H(\xi)]\alpha S_Q h/\tilde{p}\}^{1/\alpha}\, d\xi \ , \tag{30}$$

$$H(\tilde{x}_0) = \int_0^{\tilde{x}_0} G(\xi)\, d\xi \ . \tag{31}$$

In these equations, the parametric variable $\tilde{x}_0$ must be eliminated to find the spatial variation of the density field $\tilde{\rho}(\tilde{x}, \tilde{t})$. Also, Equation (28) is an implicit equation for the pressure $\tilde{p}$. Note that S_Q is the important similarity parameter in this regime.

From the above equations, it is seen that the gas density distribution at a given time is determined by the heating rate (proportional to h) at that time. By way of contrast, the amount of energy added to the gas up to that time (proportional to the time integral of h) is unimportant. Since H is monotonically increasing, Equation (29) indicates that the gas density is smallest at the center and largest at the side walls, so the heated region is optically defocusing. Moreover, this minimum becomes deeper (outward flow) as h increases and

shallower (inward flow) as h decreases. Thus, thermal-conduction effects actually worsen the spatial nonuniformity of the applied heating by increasing the density near the wall (putting more absorbers in a high-flux region) and by decreasing the density near the center (removing absorbers from a low-flux region). Note also that as $\tilde{p}$ (or equivalently S_Q) becomes large, the density field approaches a limiting profile, which is unaffected by further increasing the heat addition. Analytical results for $\tilde{u}$, $\tilde{\pi}$, and other quantities are contained in the appendix.

As an example, consider helium gas, initially at 200 kPa and 300 K, contained in a laser cell with a 1-cm gap ($L = 0.5$ cm) and with 1-μm UO_2 layers on the side walls. The heating is described by $Q_s = 2.22 \times 10^{-3}$ kW/cm^3 and $h = 1$ for $0 \leq t \leq t_D$ with $t_D = 160$ ms ($h = 0$ at other times). For this case, $S_B/S_B^* = 15$. Figures 7 and 8 show the spatial variations of the density and power density (applied heating) fields, respectively, at 80 ms and 160 ms as determined from a numerical simulation of the full equations. Neither the gas density nor

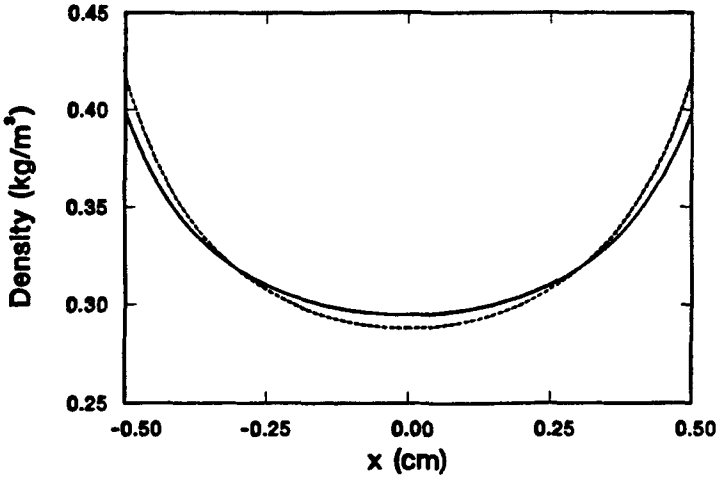

Figure 7. The density is shown as a function of position at 80 ms (solid curve) and 160 ms (dashed curve). The density field is virtually unchanged as the energy deposition increases while the power is held constant, indicating that the density field depends only on power, not energy, in the dominant-conduction regime.

the power density varies significantly when the heating is held constant.

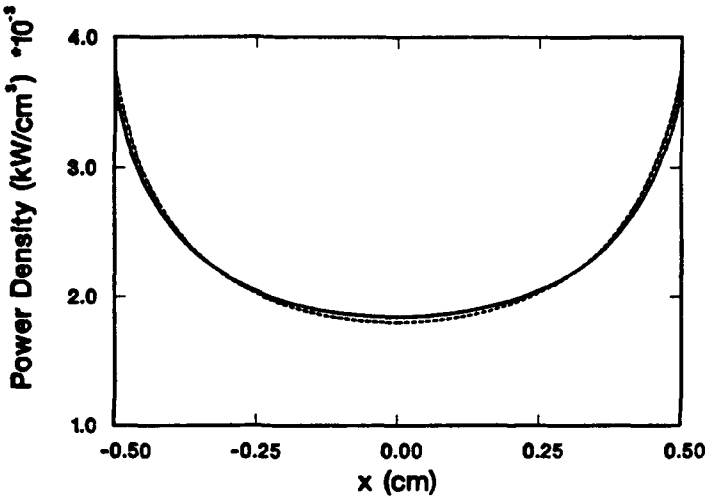

Figure 8. The power density (heating) is shown as a function of position at 80 ms (solid curve) and 160 ms (dashed curve).

The quantity $\partial^2\tilde{\rho}/\partial\tilde{x}^2(0)$ can be determined for the dominant-conduction regime. In the limit $S_B \to \infty$ with $h(\tilde{t}) = 1$, this quantity can be expressed as

$$\frac{\partial^2\tilde{\rho}}{\partial\tilde{x}^2}(0) = q_1(S_H, S_F)\, q_2(S_Q, S_H, S_F)\ . \tag{32}$$

Plots of q_1 and q_2 are given in Figures 9 and 10. These generic plots can be used to determine the amount of lensing to be expected for experiments lying in the dominant-conduction regime. From these graphs, it is seen that the curvature does not depend strongly on S_H or S_Q for S_Q above unity.

The normalized pressure $\tilde{p}$ can also be determined for the dominant-conduction regime. In the limit $S_B \to \infty$ with $h(\tilde{t}) = 1$, this quantity can be expressed as

$$\tilde{p} = p_1(S_H, S_F)\, p_2(S_Q, S_H, S_F)\ . \tag{33}$$

Plots of p_1 and p_2 are given in Figures 11 and 12. From these graphs, it is seen that S_H does not affect $\tilde{p}$ greatly. Increasing S_Q (increasing the applied heating relative to the ability of thermal conduction to remove heat) is seen to result in the expected increase in $\tilde{p}$.

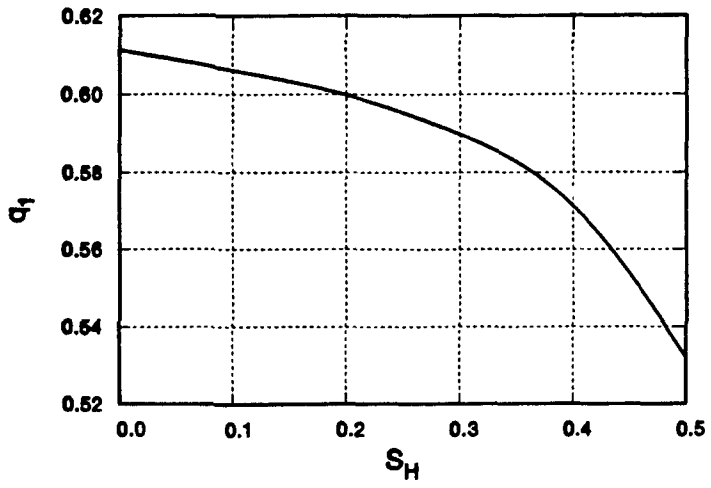

Figure 9. The quantity q_1 is plotted against S_H for $S_F = 0.2$ and $\alpha = 0.75$. These results depend very weakly on S_F.

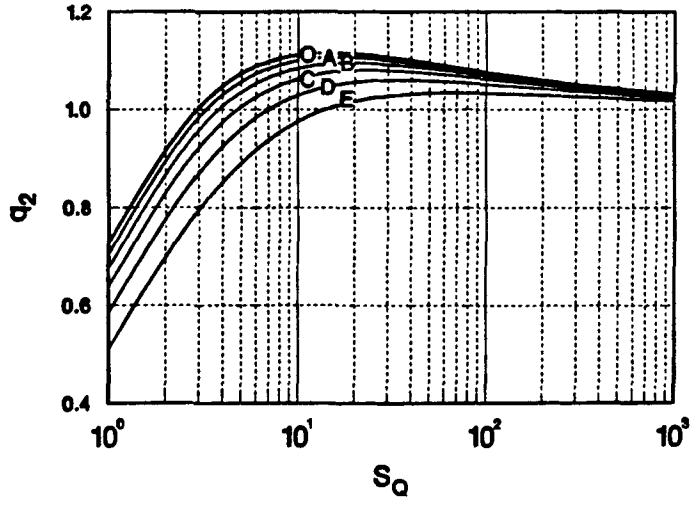

Figure 10. The quantity q_2 is plotted against S_Q for $S_F = 0.2$, $\alpha = 0.75$, and the following S_H values: $S_H = 0.0$ (curve O); $S_H = 0.1$ (curve A); $S_H = 0.2$ (curve B); $S_H = 0.3$ (curve C); $S_H = 0.4$ (curve D); $S_H = 0.5$ (curve E). These results depend very weakly on S_F.

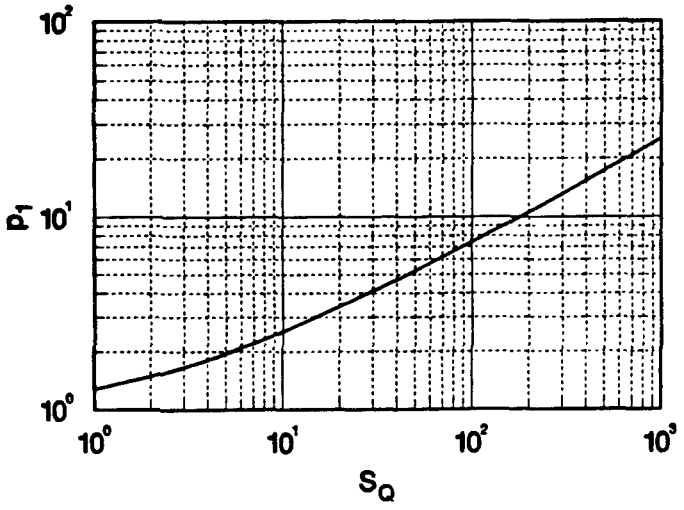

Figure 11. The quantity p_1 is plotted against S_H for $S_F = 0.2$ and $\alpha = 0.75$. These results depend very weakly on S_F.

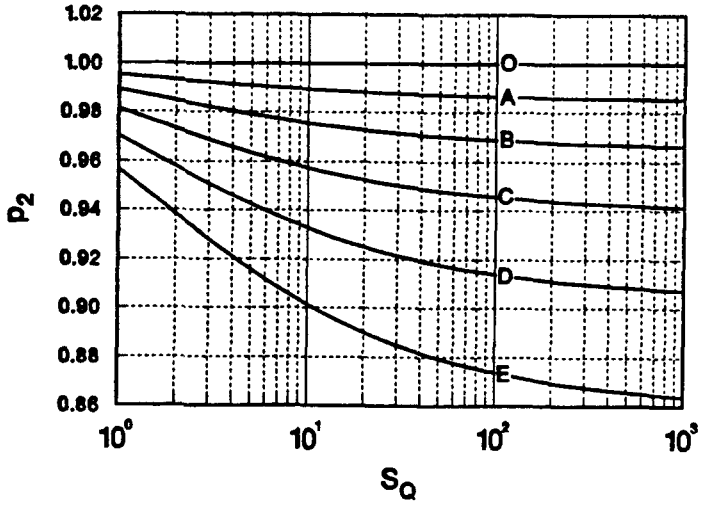

Figure 12. The quantity p_2 is plotted against S_Q for $S_F = 0.2$, $\alpha = 0.75$, and the following S_H values: $S_H = 0.0$ (curve O); $S_H = 0.1$ (curve A); $S_H = 0.2$ (curve B); $S_H = 0.3$ (curve C); $S_H = 0.4$ (curve D); $S_H = 0.5$ (curve E). These results depend very weakly on S_F.

Mixed Regime

In the mixed regime ($S_B/S_B^* \sim 1$), the competing effects of spatially nonuniform heating and thermal conduction produce a complex gas motion. No analytical solution is available, so numerical solutions of the equations of motion are necessary to study the gas flow in this regime. However, qualitative statements can be made regarding the flow based on the results of the two previous sections. Since S_B/S_B^* is the ratio of the pulse duration to the time required for the thermal boundary layers to grow from the side walls into the center, at early times the thermal boundary layers are thin, but they have reached the center of the laser cell at later times. Therefore, mixed-regime cases resemble cases in the negligible-conduction regime at early times but resemble cases in the dominant-conduction regime at later times. In a similar vein, the flow in the central region of the laser cell resembles the flow in the negligible-conduction regime, but the flow near the side walls resembles the flow in the dominant-conduction regime. Thus, the competition of thermal-conduction and heating-nonuniformity effects acts to produce both a density maximum at $x = 0$ and large densities at the side walls, with density minima at intermediate locations. These minima are quite close to the walls at early times, but they propagate in toward the center and eventually engulf the central maximum. Furthermore, this motion depends in a complex manner on both the energy, as in the negligible-conduction regime, and the power, as in the dominant-conduction regime. Note that there are both optically focusing and defocusing regions since both maxima and minima exist in the density field.

As an example, consider helium gas, initially at 200 kPa and 300 K, contained in a laser cell with a 1-cm gap ($L = 0.5$ cm) and with 1-μm UO_2 layers on the side walls. The heating is described by $Q_s = 0.089$ kW/cm^3 and $h = 1$ for $0 \le t \le t_D$ with $t_D = 4$ ms ($h = 0$ at other times). For this case, $S_B/S_B^* = 0.38$. Figures 13 and 14 show the spatial variations of the density and power density (applied heating) fields, respectively, at 2 ms and 4 ms as determined from a numerical simulation of the full equations. For cases in the mixed regime, the flow is frequently observed to reduce the density in the central region but maintain a

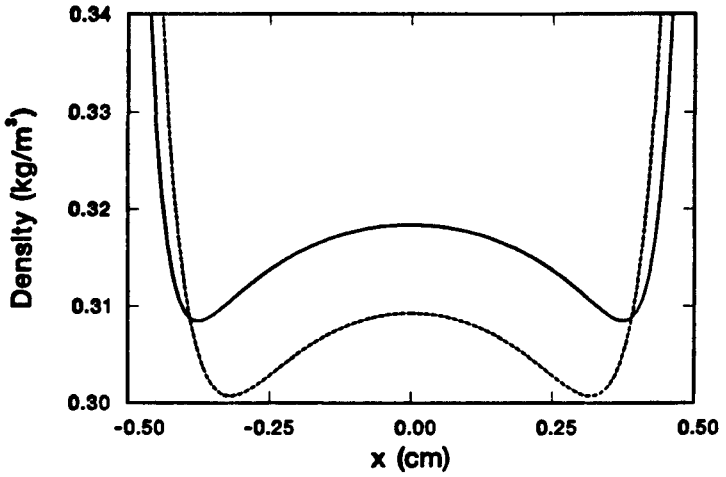

Figure 13. The density is shown as a function of position at 2 ms (solid curve) and 4 ms (dashed curve). Note the inward gas motion near the center and the outward gas motion near the walls.

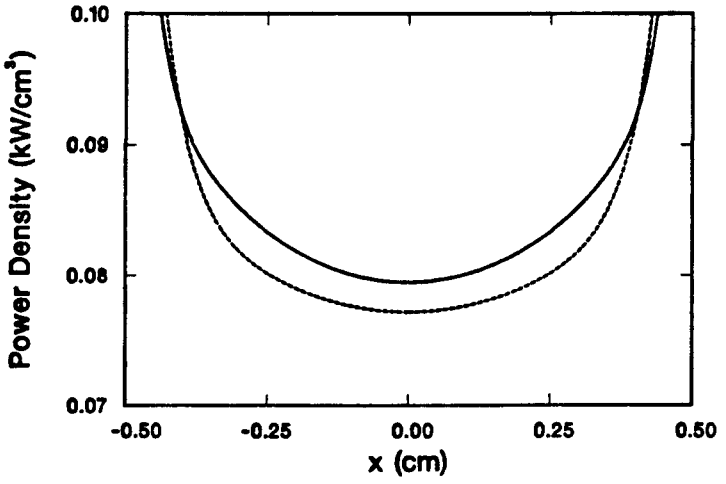

Figure 14. The power density (heating) is shown as a function of position at 2 ms (solid curve) and 4 ms (dashed curve).

roughly constant density curvature in this region while doing so.

Conclusions

A model describing the gas flow in a nuclear-reactor-pumped laser has been examined. This gas flow is induced by the competition between the spatial nonuniformity of the fission-fragment heating and the effects of thermal conduction to the side walls. Three heat-transfer and gas-flow regimes are found and characterized in terms of S_B/S_B^*, the ratio of the pulse duration to the time required for the thermal boundary layer to grow from the side walls into the center of the laser cell.

The negligible-conduction regime corresponds to small values of S_B/S_B^*. In this regime, the density field is determined solely by the energy deposited in the gas (the power is unimportant), and a central density maximum is formed (an optically focusing region). Thermal-conduction effects are confined to thin boundary layers, and little heat is removed during the pulse.

The dominant-conduction regime corresponds to large values of S_B/S_B^*. In this regime, the density field is determined solely by the power (rate of applied heating) in the gas (the energy deposited is unimportant), and a central density minimum is formed (an optically defocusing region). Thermal conduction removes heat as rapidly as it is deposited during the pulse.

The mixed regime corresponds to values of S_B/S_B^* near unity. In this regime, the density field is determined by the energy and the power. At early times, a central density maximum forms, but density minima propagate inward from the side walls and ultimately engulf the central density maximum. It is often found that the curvature of the density field in the central region remains relatively constant during the latter portion of the pulse even though the density in the central region falls significantly.

Analytical solutions of the equations were presented in the limits $S_B \rightarrow 0$ (negligible-conduction) and $S_B \rightarrow \infty$ (dominant-conduction). These solutions were used to generate graphs delineating the behavior of the curvature of the density field in terms of the relevant

dimensionless parameters.

Acknowledgments

This work was performed at Sandia National Laboratories, supported by the U. S. Department of Energy under contract number DE–AC04–76DP00789.

References

1. K. Thom and R. T. Schneider, "Nuclear Pumped Gas Lasers," *AIAA J.* **10**, 400–406 (1972).

2. D. A. McArthur and P. B. Tollefsrud, "Observation of Laser Action in CO Gas Excited Only by Fission Fragments," *Appl. Phys. Lett.* **26**, 187–190 (1975).

3. H. H. Helmick, J. L. Fuller, and R. T. Schneider, "Direct Nuclear Pumping of a Helium-Xenon Laser," *Appl. Phys. Lett.* **26**, 327–328 (1975).

4. G. H. Miley, "Direct Nuclear Pumped Lasers — Status and Potential Applications," in *Laser Interaction and Related Plasma Phenomena* **4**, edited by H. Hora and G. Miley (Plenum, New York, 1976), pp. 181–228.

5. M. A. Prelas, M. A. Akerman, F. P. Boody, and G. H. Miley, "A Direct Nuclear Pumped 1.45-μ Atomic Carbon Laser in Mixtures of He-CO and He-CO_2," *Appl. Phys. Lett.* **31**, 428–430 (1977).

6. R. J. De Young, Y. J. Shiu, and M. D. Williams, "Fission-Fragment Nuclear Lasing of Ar(He)-Xe," *Appl. Phys. Lett.* **37**, 679–6681 (1980).

7. A. M. Voinov, L. E. Dovbysh, V. N. Krivonosov, S. P. Mel'nikov, I. V. Podmoshenskii, and A. A. Sinyanskii, "Fission-Pumped He-Xe and Ar-Xe Infrared Lasers," *Sov. Tech. Phys. Lett.* **7**, 437 (1981).

8. G. N. Hays, D. A. McArthur, D. R. Neal, and J. K. Rice, "Gain Measurements Near 351 nm in $^3He/Xe/NF_3$ Mixtures Excited by Fragments from the $^3He(n,p)^3H$ Reaction," *Appl. Phys. Lett.* **49**, 363–365 (1986).

9. J. K. Rice, G. N. Hays, D. R. Neal, D. A. McArthur, and W. J. Alford, "Nuclear Reactor Excitation of XeF Laser Gas Mixtures," in *Proceedings of the International Conference on Lasers '86*, edited by R. W. McMillan (STS Press, McLean, VA, 1987), pp. 571–578.

10. D. A. McArthur, G. N. Hays, W. J. Alford, D. R. Neal, D. E. Bodette, and J. K. Rice, "Recent Results on Reactor-Pumped Laser Studies at Sandia National Laboratories," in *Laser Interaction and Related Plasma Phenomena* **8**, edited by H. Hora and G. Miley (Plenum, New York, 1988).

11. G. H. Miley, *Direct Conversion of Nuclear Radiation Energy* (American Nuclear Society, LaGrange, IL, 1970), Chaps. 3–4.

12. M. Born and E. Wolf, *Principles of Optics* (Pergamon, New York, 1980), pp. 87–98.

13. J. R. Torczynski and D. R. Neal, *Effect of Gasdynamics on Resonator Stability in Reactor-Pumped Lasers*, Sandia Report SAND88-1318, Sandia National Laboratories (1988).

14. D. R. Neal, J. R. Torczynski, and W. C. Sweatt, "Resonator Stability Effects in "Quadratic-Duct" Nuclear-Reactor-Pumped Lasers," in *Proceedings of the International Conference Lasers '88*, edited by R. C. Sze and F. J. Duarte (STS Press, McLean VA, 1989), pp. 245–252.

15. D. R. Neal, W. C. Sweatt, and J. R. Torczynski, "Resonator Design with an Intracavity Time-Varying Index Gradient," SPIE Paper 965-40, in *Current Developments in Optical Engineering III*, edited by R. E. Fischer and W. J. Smith, *SPIE Proceedings* **965**, 130–141 (1989).

16. J. R. Torczynski and R. J. Gross, "Refractive Index Gradients in Nuclear-Reactor-Pumped Lasers: Gasdynamic Effects," in *Proceedings of the International Conference on Lasers '87*, edited by F. Duarte (STS Press, McLean, VA, 1988), pp. 241–248.

17. J. R. Torczynski and R. J. Gross, "The Gasdynamics of Fission-Fragment Heating," in *Proceedings of the 1st National Fluid Dynamics Congress*, edited by C. Dalton (AIAA, Washington DC, 1988), pp. 1040–1047.

18. J. R. Torczynski and R. J. Gross, "Axis-Shielding in Cylindrical Nuclear-Reactor-Pumped Lasers," *J. Appl. Phys.* **64** (9), 4323–4328 (1988).

19. J. R. Torczynski, R. J. Gross, G. N. Hays, G. A. Harms, D. R. Neal, D. A. McArthur, and W. J. Alford, "Fission-Fragment Energy Deposition in Argon," *Nucl. Sci. Eng.* **101** (3), 280–284 (1989).

20. J. R. Torczynski, "On the Motion of a Gas Experiencing Range-Dependent Volumetric Heating," *J. Fluid Mech.* **201**, 167–188 (1989).

21. R. C. Reid, J. M. Prausnitz, and B. C. Poling, *The Properties of Gases and Liquids* (McGraw-Hill, New York, 1986), pp. 514–518, 530–531.

22. G. H. Miley and P. E. Thiess, "A Unified Approach to Two-Region Ionization-Excitation Density Calculations," *Nucl. Appl.* **6**, 434–451 (1969).

23. J. C. Guyot, G. H. Miley, and J. T. Verdeyen, "Application of a Two-Region Heavy Charged Particle Model to Noble-Gas Plasmas Induced by Nuclear Radiations," *Nucl. Sci. Eng.* **48**, 373–386 (1972).

24. A. K. Chung and M. A. Prelas, "The Transport of Heavy Charged Particles in a Cylindrical Nuclear-Pumped Plasma," *Nucl. Sci. Eng.* **86**, 267–274 (1984).

25. R. G. Rehm and H. R. Baum, "The Equations of Motion for Thermally Driven, Buoyant Flows," *J. Res. Nat. Bur. Stand.* **83** (3), 297–308 (1978).

26. S. Paolucci, *On the Filtering of Sound from the Navier-Stokes Equations*, Sandia Report SAND82–8257, Sandia National Laboratories (1982).

27. H. S. Carslaw and J. C. Jaeger, *Conduction of Heat in Solids* (Oxford, New York, 1986), p. 61.

28. C. M. Bender and S. A. Orszag, *Advanced Mathematical Methods for Scientists and Engineers* (McGraw-Hill, New York, 1978), pp. 83–88.

Appendix

This appendix contains a compilation of analytical results relating to gas motion in the negligible-conduction and dominant-conduction regimes.

The following are analytical results for $\tilde{u}$, $\tilde{\pi}$, $\tilde{Q} = Q/Q_s$, and the density curvature in the limit $S_B \to 0$:

$$\tilde{u} = -\frac{S_A h}{\gamma \tilde{p}}[\tilde{x} - G(\tilde{x}_0)] \,, \tag{A1}$$

$$\tilde{\pi} = \left\{-\frac{d^2}{d\tilde{t}^2}\tilde{p}^{-1/\gamma}\right\}\left\{-(1-\tilde{p}^{-1/\gamma})\int_0^1 [\xi - G(\xi)]^2\, d\xi \right.$$
$$\left. - \int_0^1 (1-\xi)[\xi - G(\xi)]\, d\xi + \int_0^{\tilde{x}_0} [\xi - G(\xi)]\, d\xi \right\} \,, \tag{A2}$$

$$\tilde{Q} = hG'(\tilde{x}_0)\tilde{\rho} \,, \tag{A3}$$

$$\frac{\partial^2 \tilde{\rho}}{\partial \tilde{x}^2}(0) = -\frac{(1-\tilde{p}^{-1/\gamma})G'''(0)}{\{G'(0) + [1-G'(0)]\tilde{p}^{-1/\gamma}\}^4} \,. \tag{A4}$$

Parametric expressions for the density field $\tilde{\rho}(\tilde{x})$ are given below in the limit $S_A \to \infty$:

$$\tilde{\rho} \to [G'(\tilde{x}_0)]^{-1} \,, \tag{A5}$$

$$\tilde{x} \to G(\tilde{x}_0) \,. \tag{A6}$$

This limiting field is to be interpreted as a bound on the motion rather than as a physically realizable field.

The following are analytical results for $\tilde{u}$, $\tilde{\pi}$, $\tilde{Q} = Q/Q_s$, and the density curvature in the limit $S_B \to \infty$:

$$\tilde{u} = \left\{\frac{S_Q}{\tilde{p}^2}\frac{dh}{d\tilde{t}}\right\}\left\{I(\tilde{x}_0) - I(1)\left[\frac{\tilde{p}^2\tilde{x} + hI(\tilde{x}_0)}{\tilde{p}^2 + hI(1)}\right]\right\} \,, \tag{A7a}$$

$$I(\tilde{x}_0) = \int_0^{\tilde{x}_0} \{1 + [H(1) - H(\xi)]\alpha S_Q h/\tilde{p}\}^{-1+1/\alpha} \times [H(1) - H(\xi)]\, d\xi \ , \tag{A7b}$$

$$\tilde{\pi} = \left(\frac{\mu_0 c_p}{\gamma k_0}\right)\left(\frac{4}{3}\tilde{\mu} + \tilde{\mu}_v\right) \times \left\{\tilde{\rho} J(\tilde{x}_0) - I(1)\left[\frac{\tilde{p}^2 + h\tilde{\rho} J(\tilde{x}_0)}{\tilde{p}^2 + hI(1)}\right]\right\} \ , \tag{A8a}$$

$$J(\tilde{x}_0) = \{1 + [H(1) - H(\tilde{x}_0)]\alpha S_Q h/\tilde{p}\}^{-1+1/\alpha} \times [H(1) - H(\tilde{x}_0)] \ , \tag{A8b}$$

$$\tilde{Q} = hG'(\tilde{x}_0)\tilde{\rho} \ , \tag{A9}$$

$$\frac{\partial^2 \tilde{\rho}}{\partial \tilde{x}^2}(0) = \frac{S_Q h \tilde{p}^2 G'(0)}{[1 + H(1)\alpha S_Q h/\tilde{p}]^{1+3/\alpha}} \ . \tag{A10}$$

Parametric expressions for the density field $\tilde{\rho}(\tilde{x})$ in the limit $S_Q \to \infty$:

$$\tilde{\rho} \to \frac{\int_0^1 [H(1) - H(\xi)]^{1/\alpha}\, d\xi}{[H(1) - H(\tilde{x}_0)]^{1/\alpha}} \ , \tag{A11}$$

$$\tilde{x} \to \frac{\int_0^{\tilde{x}_0} [H(1) - H(\xi)]^{1/\alpha}\, d\xi}{\int_0^1 [H(1) - H(\xi)]^{1/\alpha}\, d\xi} \ . \tag{A12}$$

This limiting field is to be interpreted as a bound on the motion rather than as a physically realizable field. Note that this density field has an integrable singularity at $\tilde{x} = \tilde{x}_0 = 1$.

In these derivations, frequent use has been made of the fact that

$$\tilde{\rho}\left(\frac{\partial \tilde{x}}{\partial \tilde{x}_0}\right)_{\tilde{t}} = 1 \ , \tag{A13}$$

which is the equation of continuity written in Lagrangian form.